Carbohydrate Polymers 271 (2021) 118409

Contents lists available at ScienceDirect

Carbohydrate Polymers

journal homepage: www.elsevier.com/locate/carbpol

Valorization of *Larix decidua* Mill. bark by functionalizing bioextract onto chitosan films for sustainable active food packaging

Charu Agarwal [a,*], Zsófia Kóczán [b], Zoltán Börcsök [a], Katalin Halász [b], Zoltán Pásztory [a]

[a] Innovation Center, University of Sopron, Bajcsy-Zsilinszky E. str. 4, Sopron 9400, Hungary
[b] Paper Research Institute, University of Sopron, Bajcsy-Zsilinszky E. str. 4, Sopron 9400, Hungary

ARTICLE INFO

Keywords:
Active packaging
Chitosan film
Polyphenolic antioxidants
Larch bark

ABSTRACT

The present study explored the use of chitosan films functionalized with antioxidants extracted from *Larix decidua* Mill. bark for active packaging. The pristine chitosan and extract-incorporated chitosan films were evaluated for their structural, physico-mechanical, thermal, viscoelastic and antioxidant properties using advanced characterization techniques. The infrared spectroscopy revealed hydrogen bonding between the extract polyphenolic antioxidants and chitosan, whereas the surface microscopy studies indicated good compatibility between them. The addition of bark extract caused a significant increase in color parameters and solubility with reduction in swelling and elongation at break of the films. The thermal analysis indicated a drop in thermal stability of chitosan films modified with the extract. The dynamic mechanical analysis confirmed the extract-polymer interactions and the viscoelastic nature of the films. The incorporation of bark extract caused remarkable enhancement in the antioxidant activity of chitosan films. Overall, larch bark extract-functionalized chitosan films demonstrated promising potential for food packaging.

1. Introduction

Global hunger is a key issue facing humanity- an estimated 2 billion people world over did not have regular access to nutritious, safe and sufficient food while, 750 million people were exposed to severe levels of food insecurity in 2019 (FAO et al., 2020). While food production can be adopted as a measure to resolve the issue, a food loss reduction strategy would be the most sustainable alternative to achieving food security. This can be understood from an alarming fact that one-third of all food is either wasted or lost annually (FAO, 2021). The Food and Agriculture Organization has pointed the instrumental role of packaging in preventing food wastage to ensure food security and safety (FAO, 2014). Petroleum-derived plastics constitute a huge chunk (42%) of the materials used for packaging, posing immense threat to the ecosystem due to their non-biodegradable nature (Jeevahan & Chandrasekaran, 2019). To address these challenges, there is a pressing need for finding effective packaging solutions that will assist not only in minimizing the food loss but also in alleviating the carbon footprint.

The past few decades have witnessed significant efforts in pursuit of biodegradable packaging to meet the global demand for sustainability. Various polysaccharides and proteins of natural origin have been investigated as alternative materials for packaging on account of their wide availability, biodegradability, biocompatibility, renewability, non-toxicity and low-cost (Zhong et al., 2020). Despite several advantages, the industrial applicability of biopolymers is limited mainly due to their poor barrier and mechanical properties. Chitosan, one of the most abundant biopolymers obtained from chitin, is well-known for its anti-microbial property and eco-friendliness (Kalaycıoğlu et al., 2017). In addition, it has an excellent film-forming ability with good mechanical resistance and edible characteristics, thus making chitosan an attractive material for food packaging (Jeevahan & Chandrasekaran, 2019; Sun et al., 2017). However, the low antioxidant activity of chitosan film cannot meet the standards of active packaging (Yong et al., 2019). Thus, functionality of chitosan needs to be enhanced to curtail food spoilage, which is primarily caused by microbial growth and oxidative degradation (Vilela et al., 2018).

Incorporating antioxidants into packaging materials can help in maintaining food quality over time, thus extending its shelf life. Lately, research on natural additives has picked up greatly owing to the adverse effects of synthetic chemicals, consumer awareness and environmental concerns (Lourenço et al., 2019). Secondary metabolites from plants such as polyphenols can act as free radical scavengers or oxygen

* Corresponding author.
E-mail address: charu.agarwal3@gmail.com (C. Agarwal).

https://doi.org/10.1016/j.carbpol.2021.118409
Received 31 March 2021; Received in revised form 1 July 2021; Accepted 3 July 2021
Available online 8 July 2021

quenchers, thereby delaying oxygen-triggered undesirable reactions in food (lipid peroxidation, protein denaturation and enzymatic browning) that result in lower nutritional value, color deterioration and off-flavors (Lourenço et al., 2019; Sanches-Silva et al., 2014; Vilela et al., 2018). Natural antioxidants extracted from plants like rosemary, tea, ginger, as well as a variety of essential oils have been explored in active packaging (Souza et al., 2017). Particularly, secondary biomass (processing wastes and residues) such as olive pomace, mango kernel, thinned apples, potato peels, garlic husk, rice bran, etc., have generated immense interest in active packaging due to their high content of bioactive compounds (Etxabide et al., 2017; Lourenço et al., 2019; Sun et al., 2017).

The tree bark is a forest byproduct rich in phenolic compounds with a vast potential for valorization. Our earlier study found significant antioxidant capacity of bark extracts from popular trees in Europe (Agarwal, Hofmann, Visi-Rajczi, & Pásztory, 2021). The European larch (*Larix decidua* Mill.), a deciduous conifer spread across central Europe, is of industrial value and its constituents find use in folk medicine (Baldan et al., 2017). In this work, we incorporated polyphenolic antioxidants from the European larch bark into chitosan films with an aim to investigate the compatibility between them for their suitability in active packaging. Larch bark extract-functionalized chitosan (LEC) films were developed using a facile method and extensively characterized using advanced analytical instruments to compare their structural, optical, physico-mechanical, thermal, viscoelastic and antioxidant properties with those of pristine chitosan (PC) film. As far as we know, the incorporation of tree bark extract into chitosan films for active packaging has not been reported before. The work is expected to be a significant contribution towards the development of sustainable materials for active food packaging.

2. Materials and methods

2.1. Materials

Chitosan with degree of deacetylation of 80% and viscosity of 20–100 mPa·s (0.5% in 0.5% acetic acid at 20 °C) was procured from TCI, Hungary. Folin-Ciocalteu's phenol reagent (2 N), 2,2-diphenyl-1-picrylhydrazyl (DPPH) free radical, sodium carbonate and gallic acid were procured from Sigma-Aldrich, Hungary. Methanol, ethanol, glycerol and acetic acid were obtained from Molar Chemicals Ltd., Hungary. All the chemicals were of analytical grade and used as received. Deionized water was used for making the standard solutions and dilutions.

Whole bark of *Larix decidua* Mill. was collected from the forests of Sopron (Hungary) in December 2019. The samples were subsequently air-dried, ground (0.2–0.63 mm) and stored in plastic bags in the freezer at −20 °C.

2.2. Preparation of larch bark extract

The extraction of bioactive compounds from larch bark was done according to our earlier method (Agarwal, Hofmann, Visi-Rajczi, & Pásztory, 2021). Briefly, bark specimen (2 g) was treated in 80% aqueous ethanol solution (75 mL) for 15 min at full amplitude using an ultrasonic probe sonicator (Tesla 150 WS) operating at 20 kHz frequency. The temperature during sonication was about 74 °C. The extract was cooled and filtered with filter paper, 12.5 cm in diameter (Macherey-Nagel, Düren, Germany). It was stored in dark glass bottles in the freezer at −20 °C.

2.3. Preparation of films

The methodology for making the films was adapted from earlier studies, with some modifications (Halász & Csóka, 2018; Kaya et al., 2018). Chitosan solution of 1 wt% was prepared by dissolving chitosan powder in 1 mg/mL acetic acid solution for 2 h on a magnetic stirrer at room temperature (20 ± 2 °C). Larch bark extract was mixed with the chitosan solution with gentle stirring for 10 min at room temperature using glycerol (20 wt%, based on dry weight of chitosan) as a plasticizer. The films were made by casting the mixture into plastic trays after treating it under vacuum to prevent any bubble formation in the film structure. They were allowed to air-dry at 20 ± 2 °C in ambient conditions for 4 days. Finally, the films were pulled off the trays and stored in plastic bags, away from light. Pristine chitosan (control) films were made in a similar fashion without the extract. The films were coded as PC, LEC-3, LEC-6 and LEC-9 for pristine chitosan, 3 wt%, 6 wt% and 9 wt % extract concentration (based on weight of the film-forming solution), respectively. Three films were made for the control and each extract concentration to perform the analyses in triplicate.

2.4. Structural characterization

2.4.1. Scanning electron microscopy (SEM)

The SEM images of the film microstructure were obtained using Hitachi S-3400 N scanning electron microscope (Tokyo, Japan) at an accelerating voltage of 10 kV. Prior to imaging, the film specimens were coated with Au/Pd for 60 s on a sputter coater (SC7620, Quorum Technologies Ltd., UK). The surface and cross-section micrographs were recorded at magnifications of 1000× and 1500×, respectively (J. Liu et al., 2017).

2.4.2. Atomic force microscopy (AFM)

The AFM imaging of the chitosan films was done using Omegascope I/O007 (Horiba France SAS, France) in ambient environment, in tapping mode (Ferreira et al., 2014). A pyramidal silicon tip (MikroMasch NSC14/Al BS) with a force constant of 5.0 N/m and a resonance frequency of 160 kHz was used. The scan rate was 1 Hz on a scan area of 500 × 500 nm^2. Two and three-dimensional (3D) topography and phase images of the films were acquired on scanning probe microscopy platform (Horiba Scientific–AIST-NT). The root mean square (RMS) surface roughness was calculated based on the deviation from the average peak heights after subtracting the background using Gwyddion 2.57 software.

2.4.3. Fourier-transform infrared (FTIR) spectroscopy

The FTIR spectra were collected using Jasco FT/IR 6300 spectrophotometer (Tokyo, Japan) equipped with an ATR PRO 470-H. The spectra were recorded in the range of 4000 to 500 cm^{-1} in the transmission mode with 32 scans per film specimen and a resolution of 4 cm^{-1} at ambient conditions (Halász & Csóka, 2018).

2.5. Optical properties

2.5.1. Color

The film color was determined by measuring CIE-L*a*b* coordinates, where L* indicated lightness (100) or darkness (0), a* indicated redness (+) or greenness (−), and b* indicated yellowness (+) or blueness (−), with Datacolor Elrepho 2000 spectrophotometer (Zürich, Switzerland). The tests were done using D65 illuminant/10° observer against a white background standard. The total color difference of LEC films with respect to PC film (Δ*E*), chroma and hue were calculated using Eqs. (1)–(4), respectively (Halász & Csóka, 2018; Souza et al., 2017). Values were expressed as the means of three measurements at random points on each film, with three replicates per type of film.

$$\Delta E = \left(\left(L_i^* - L^*\right)^2 + \left(a_i^* - a^*\right)^2 + \left(b_i^* - b^*\right)^2 \right)^{1/2} \quad (1)$$

where, L_i^*, a_i^* and b_i^* are the color parameters of the film to be compared.

$$chroma = \left(a^{*2} + b^{*2}\right)^{1/2} \quad (2)$$

$$hue = arctan\left(\frac{b^*}{a^*}\right) (if\ a^* > 0)\ or \tag{3}$$

$$hue = arctan\left(\frac{b^*}{a^*}\right) + 180°(if\ a^* < 0) \tag{4}$$

2.5.2. Opacity

The film opacity was determined by measuring the absorbance of a specimen at 600 nm on UV/VIS spectrophotometer (WPA Lightwave S2000, UK) using Eq. (5), according to an earlier method (Park & Zhao, 2004).

$$Opacity\ (mm^{-1}) = \frac{Film\ absorbance\ at\ 600\ nm}{Film\ thickness\ (mm)} \tag{5}$$

2.6. Physical properties

2.6.1. Thickness

The film thickness was measured at five random points on each specimen using Lorentzen & Wettre 221 digital micrometer (Stockholm, Sweden), having a precision of 0.001 mm.

2.6.2. Density

The film density was calculated from its weight, area and thickness using Eq. (6), based on a previous method (Siripatrawan & Harte, 2010).

$$Density\ (g/cm^3) = \frac{Film\ weight\ (g)}{Film\ area\ (cm^2) \times thickness\ (cm)} \tag{6}$$

2.6.3. Moisture content, swelling and solubility

The moisture content, swelling and solubility were determined according to previous protocols with some modifications (Peng et al., 2013; Souza et al., 2017). The film specimen of 1.5 × 1.5 cm^2 was weighed to the nearest precision of 0.0001 g on Sartorius A200S analytical balance (Göttingen, Germany) to give the initial weight (w_1). The specimen was dried in an oven (VEB Labortechnik Ilmenau, Germany) at 70 °C for 24 h to give the dry weight (w_2). Next, the specimen was immersed in 25 mL of deionized water in a Petri dish, covered and kept at room temperature. After 24 h, the specimen was removed, superficially dried by absorbing the excess water on blotting paper and weighed to give the swollen weight (w_3). The swollen specimen was dried in the oven at 70 °C for 24 h and weighed to give the final weight (w_4). The moisture content, swelling and solubility were calculated using Eqs. (7)–(9), respectively.

$$Moisture\ content\ (\%) = \frac{w_1 - w_2}{w_1} \times 100 \tag{7}$$

$$Swelling\ (\%) = \frac{w_3 - w_2}{w_2} \times 100 \tag{8}$$

$$Solubility\ (\%) = \frac{w_2 - w_4}{w_2} \times 100 \tag{9}$$

2.6.4. Water vapor permeability (WVP)

The water vapor transmission through the films was tested using the water method, according to ASTM E96 standard (ASTM International, 2016). Briefly, a circular film specimen was cut and sealed to a test dish containing distilled water (100% relative humidity). After weighing, the dish was placed in a desiccator containing silica gel kept in a climate chamber at 20 °C. The drop in weight was recorded periodically for 7 days. Two film specimens of each type of film were analyzed and WVP was determined using Eq. (10).

$$WVP\ (g\ s^{-1}\ m^{-1}\ Pa^{-1}) = \frac{G \times t}{T \times A \times \Delta p} \tag{10}$$

where, G is the weight change (g), t is the film thickness (m), T is the time (s), A is the exposed area (m^2), Δp is the vapor pressure difference (Pa).

2.7. Mechanical properties

The mechanical strength of the films was assessed by measuring the tensile strength and elongation at break on Instron 3345 tensile tester (Norwood, USA) (Halász & Csóka, 2018). Before testing, the films were conditioned at 23 °C and 50% RH for 24 h. The measurements were done on three replicates of each film (10 mm × 125 mm), with 20 mm/min crosshead speed and 40 mm gauge length. The tensile strength and elongation at break of the films were determined using Eqs. (11)–(12) (Yong et al., 2019).

$$Tensile\ strength\ (MPa), \sigma = \frac{F}{t \times w} \tag{11}$$

$$Elongation\ at\ break\ (\%), E = \frac{\Delta L}{L} \times 100 \tag{12}$$

where, F is the maximum load applied for film fracture (N), t is the film thickness (mm), w is the film width (mm), ΔL and L are the elongated and initial film lengths (mm), respectively.

2.8. Thermo-gravimetric (TG) and differential scanning calorimetry (DSC) analyses

The simultaneous TG-DSC analyses of films were performed on Labsys evo STA 1150 (Setaram, France). About 12–16 mg of film specimen was placed in an alumina pan and heated from ambient temperature to 800 °C at 20 °C/min under nitrogen atmosphere (50 mL/min flowrate) (Kalaycıoğlu et al., 2017). An empty alumina pan was used as the reference.

2.9. Dynamic mechanical analysis (DMA)

The DMA was performed with DMA 50 (ACOEM Metravib, France) according to an earlier procedure (Assis et al., 2020). One specimen of each type of film of size around 15 × 25 mm was analyzed according to the following parameters: frequency of 1 Hz, amplitude of 20 μm, force of 1 N, and heating rate of 3 °C/min from 25 to 250 °C.

2.10. Antioxidant properties

2.10.1. Total phenol content (TPC)

For the TPC assay, film extract was prepared by dissolving 25 mg of the specimen in 10 mL of aqueous ethanol (50%), according to a previous method with some modifications (Siripatrawan & Harte, 2010). In a typical test, 1 mL of the film extract was mixed with 2.5 mL of Folin-Ciocalteu's reagent (10-fold diluted) in a test-tube. After 1 min, 2 mL of sodium carbonate solution (0.7 M) was added to the reaction mixture, and it was kept in a hot-water bath at 50 °C for 5 min. Absorbance was recorded at 760 nm on UV-VIS spectrophotometer with blank solution as the reference. Gallic acid was used as a calibration standard and the results were expressed in mg equivalents of gallic acid/g dry weight of film (mg GAE/g dw).

2.10.2. DPPH radical scavenging assay

For the DPPH assay, a standard solution of DPPH (2×10^{-4} M) was prepared in methanol, as in our earlier method (Agarwal, Hofmann, Visi-Rajczi, & Pásztory, 2021). Absorbance values at 515 nm were measured at different dilutions for plotting the calibration graph. In a typical run, 0.4 mL of film extract was diluted with 1 mL of unbuffered methanol, followed by the addition of 2 mL of DPPH solution. The test-tube was incubated at ambient temperature in the dark for 30 min and the drop in absorbance was recorded at 515 nm. The DPPH radical scavenging activity (inhibition of free radical in percentage) was

calculated using Eq. (13), as described (Rambabu et al., 2019).

$$DPPH\ radical\ scavenging\ activity\ (\%) = \frac{A_{DPPH} - A_{ext}}{A_{DPPH}} \times 100 \quad (13)$$

where, A_{DPPH} is the absorbance of DPPH solution at 515 nm, and A_{ext} is the absorbance of the film extract at 515 nm.

2.11. Statistical analysis

All the tests were performed in triplicate unless otherwise mentioned, and the results were expressed as the mean ± standard deviation. The one-way analysis of variance and Tukey HSD test were performed using Statistica 13 (TIBCO Software Inc., USA) at a significance level of 5% ($p < 0.05$). The statistical data analysis was done using OriginPro 2018 (OriginLab Corporation, USA) and Excel 2016 (Microsoft Corporation, USA).

3. Results and discussion

3.1. SEM analysis

The effect of bark extract on the microstructure of the chitosan films was studied using electron microscopy. Fig. 1 shows the surface and cross-section micrographs of pristine and modified films obtained using SEM. The surface of the control film (Fig. 1a) appeared slightly rough, which may be attributed to the high viscosity of the chitosan solution (Liu et al., 2017). In contrast, the films incorporated with the extract showed smoother and more uniform surfaces (Fig. 1c, e and g), indicating homogenous mixing of chitosan, extract and glycerol in the film. The extract did not drastically alter the surface morphology of pristine chitosan film, which suggested a good compatibility between them. The cross-section of the control film (Fig. 1b) revealed a fractured network, probably due to the presence of crystalline and ordered regions (Talón et al., 2017). The addition of the extract clearly shows an increase in the cross-section density leading to a denser and more compact cross-section (Fig. 1d, f and h) resulting from the polymer-phenolic interactions. Similar observations have also been reported earlier (Rambabu et al., 2019).

3.2. AFM analysis

The surface topography and phase analysis of chitosan films was done using AFM, as shown in Fig. 2. The PC film exhibited rough surface and a hill-valley structure as illustrated in its 2D surface and 3D topography, respectively, with RMS roughness of 24.81 nm. Its 3D phase image showed a single phase of chitosan mixed with plasticizer. On functionalization with bark extract, the well-distributed hills and valleys disappeared, which suggested that the extract had modified the surface topography of the films. The LEC-3 film showed a smoother, yet an irregular surface with RMS roughness of 17.74 nm. Its phase image revealed a uniform distribution of the extract across the chitosan matrix. Similarly, LEC-6 film also depicted a somewhat irregular surface with RMS roughness of 23.00 nm. The nanostructures or agglomerates seen in the topography image of LEC-6 may have been a consequence of the drag force caused by solvent migration during film drying. Its phase image showed that the extract was not dispersed throughout the film. In contrast, LEC-9 film had flat regions along with deflection areas with RMS roughness of 26.88 nm. However, it showed a more or less uniform distribution of the extract in chitosan. Overall, the extract helped in maintaining the structural integrity of chitosan films with quite a homogenous distribution within the polymer matrix, implying good compatibility between the two, which was also established with SEM study.

3.3. FTIR analysis

The intermolecular interactions between larch bark extract and chitosan were revealed with the help of infrared spectroscopy. As shown in Fig. 3, the FTIR spectra of pristine chitosan exhibited a broad band around 3000–3500 cm^{-1} corresponding to –OH stretching vibration overlapping with –NH symmetric stretching (Yong et al., 2019). Characteristic bands obtained at 2925 cm^{-1} and 2877 cm^{-1} corresponded to C—H stretching (Sun et al., 2017). Amide group bands were obtained at 1630 cm^{-1} (C═O stretching of amide I), 1540 cm^{-1} (N—H bending of amide II), and 1336 cm^{-1} (C—N stretching of amide III) (Ferreira et al., 2014; Kalaycıoğlu et al., 2017). A prominent band at 1403 cm^{-1} was due to $–CH_2$ bending and $–C–CH_3$ deformation (Halász & Csóka, 2018), while the bands at 1153 cm^{-1} and 1063 cm^{-1} were assigned to C–O–C asymmetric stretching and C—O stretching, respectively (Halász & Csóka, 2018; Yong et al., 2019).

After incorporation of the extract, very similar spectra were obtained with no significant wavelength shifts or changes in band intensity, indicating that no covalent interaction occurred between the extract polyphenols and chitosan. Hydrogen bonding may have formed between the –OH groups of polyphenols with –OH or –NH groups of chitosan contributing to physical interactions between them (Sun et al., 2017). This may have resulted in internal bond changes in some functional groups, which was reflected in the bands at 2877 cm^{-1} and 1630 cm^{-1} becoming less discernible with increasing extract concentration. Further, no additional bands characteristic to polyphenols were observed possibly due to the low amounts of the phenolic groups, also found in other studies (Talón et al., 2017; Yong et al., 2019).

3.4. Optical analysis

The color and opacity of chitosan films modified with larch bark extract by CIE-L*a*b* method are given in Table 1. Visually, PC film was transparent and LEC films were brownish in color. The color changes in modified films can be attributed to the ability of the extract constituents to structurally bind with chitosan (Souza et al., 2017). Addition of the extract significantly affected ($p < 0.05$) the color parameters of the films. With increasing extract concentration, the lightness (L*) of the films decreased, while the redness (+a*) and yellowness (+b*) increased. The total color difference of LEC films compared to PC film significantly increased ($p < 0.05$) with incorporation of the extract, as indicated by ΔE values. Similar effects were observed on blending *Nigella sativa* seed phenolic extract into chitosan films (Kadam et al., 2018). The chroma rose sharply from 4.56 to 42.29, and the hue dropped from 94.61 to 67.84, for PC and LEC-9, respectively. The opacity of the films showed a rising trend from 2.21 for PC to 6.64 for LEC-9, although the differences were not significant ($p > 0.05$). Higher opacity is a desirable property of food packaging materials, as it blocks the radiation that catalyzes oxidation causing food deterioration (Souza et al., 2017). Other studies incorporating phytoextracts into chitosan have also reported color and opacity trends in accordance with the observations in this work (Rambabu et al., 2019; Siripatrawan & Harte, 2010).

3.5. Physico-mechanical analysis

The physical and mechanical properties of chitosan films are shown in Table 2. No significant differences ($p > 0.05$) were found in the thickness of PC and LEC films that showed an average film thickness of 0.062 mm. This suggested that bark polyphenols could be well distributed in the chitosan matrix, even at high extract content. The density of chitosan films depicted an increasing trend with the extract content from 0.65 g/cm^3 for PC to 1.38 g/cm^3 for LEC-9, although not significantly ($p > 0.05$). The rise in density of chitosan films with extract content could be caused by greater polyphenol-polymer interactions, leading to tighter binding between them and a more compact film structure. Similar observations have been reported for young apple polyphenols (Sun et al.,

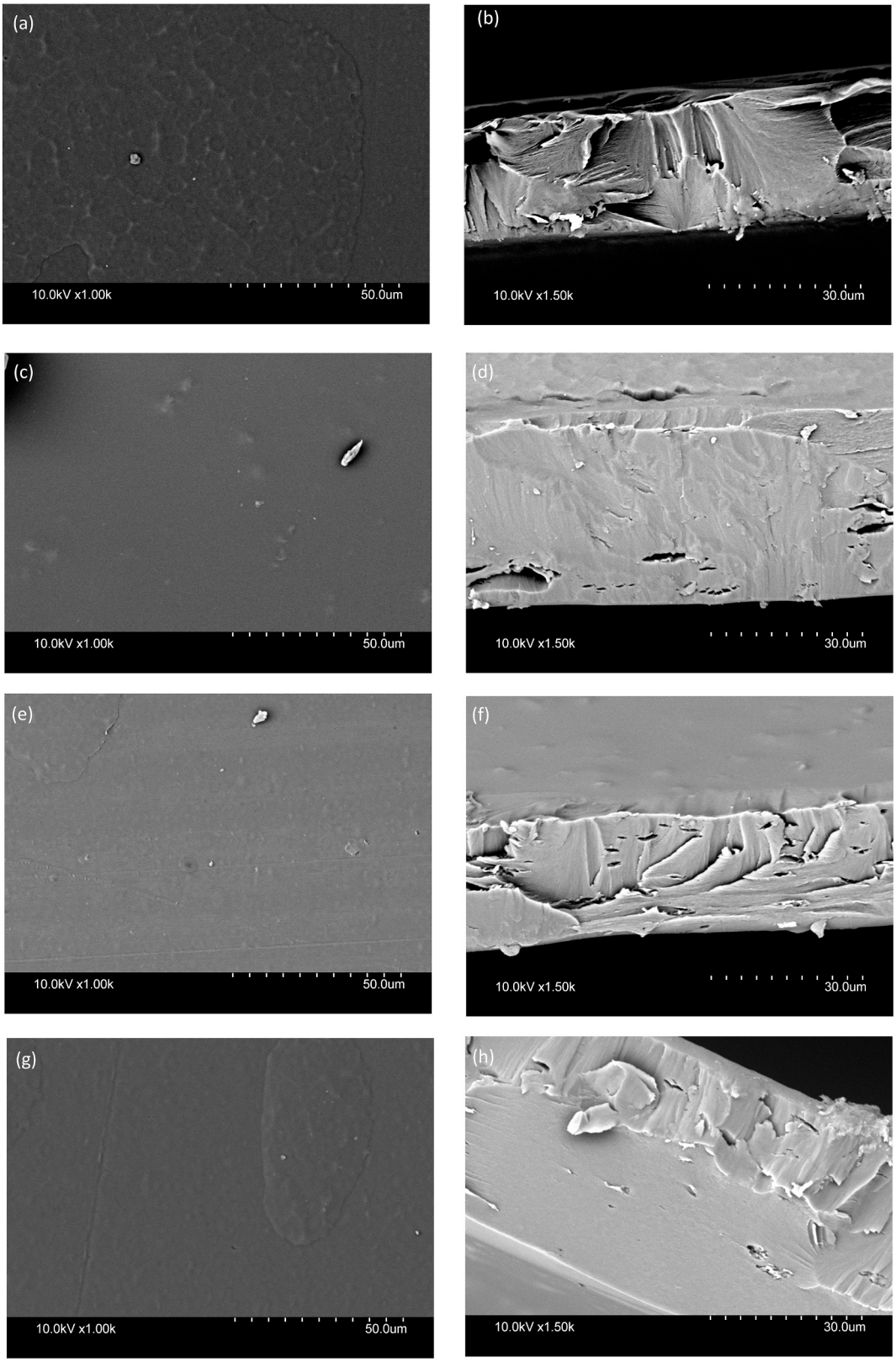

Fig. 1. SEM micrographs of surfaces (left) and cross-sections (right) of pristine chitosan (a, b); LEC-3 (c, d); LEC-6 (e, f) and LEC-9 (g, h) films. LEC-3, LEC-6 and LEC-9 represent chitosan films with 3 wt%, 6 wt% and 9 wt% larch bark extract concentration, respectively.

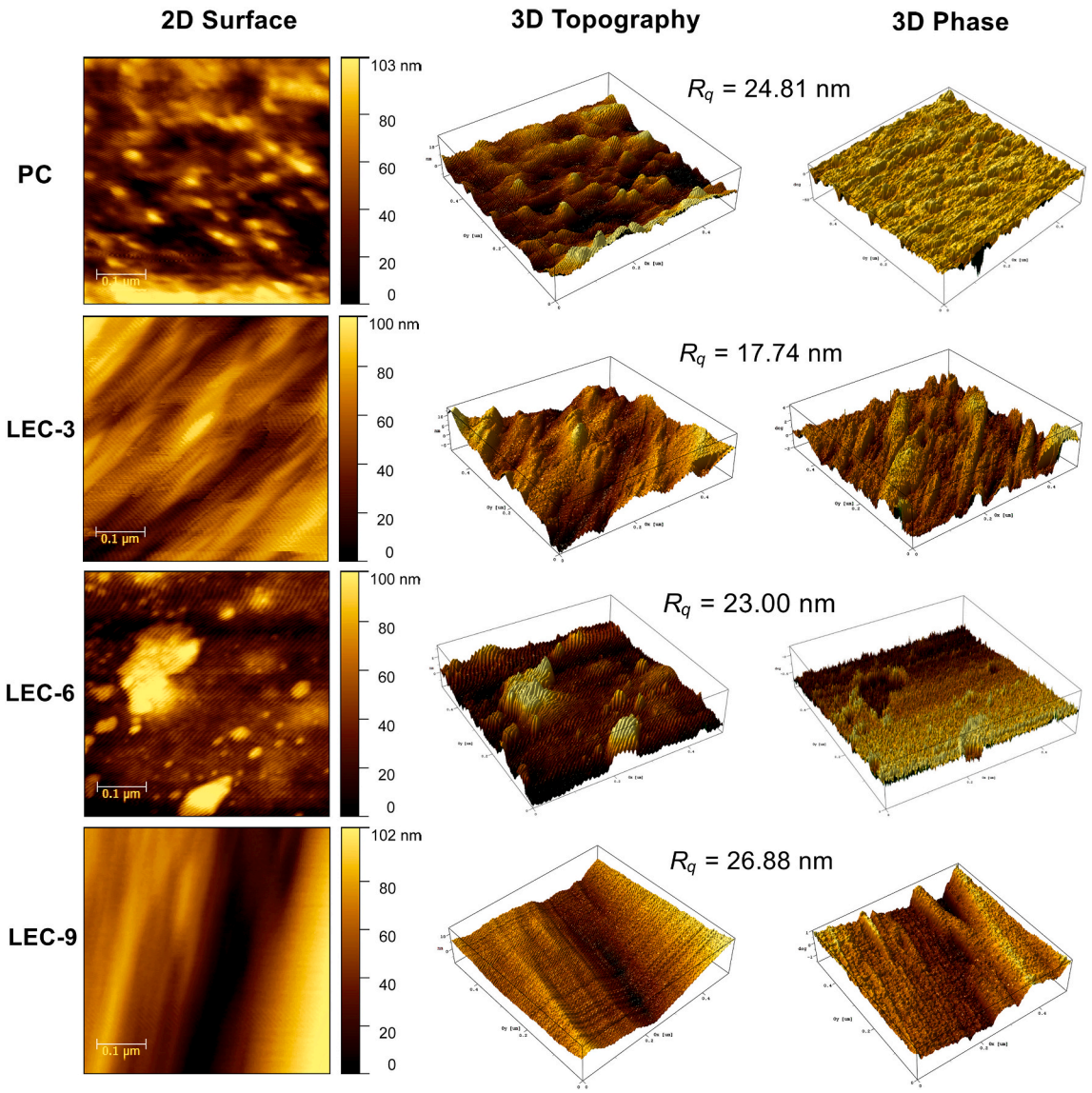

Fig. 2. AFM micrographs showing 2D surface (left), 3D topography (middle) and 3D phase (right) of pristine chitosan (PC) and larch bark extract-functionalized films with their RMS surface roughness (R_q) values. LEC-3, LEC-6 and LEC-9 represent chitosan films with 3 wt%, 6 wt% and 9 wt% larch bark extract concentration, respectively.

2017) and green tea extract (Siripatrawan & Harte, 2010) incorporated into chitosan.

The moisture content, swelling and solubility are vital indicators of water resistance property of a packaging material. The moisture content decreased significantly ($p < 0.05$) from 14.69% for PC to 10.29% for LEC-9. The relatively lower moisture content of LEC films could have resulted from the intermolecular hydrogen bonding between the –OH groups of polyphenols and –OH/–NH_2 groups of chitosan, thus limiting the chitosan-water interactions due to competitive binding effect (Wang et al., 2019; Yong et al., 2019). Swelling and solubility showed opposite trends on films incorporated with bark extractives. The swelling degree dropped significantly ($p < 0.05$) by 92%, from 2752% for PC to 217% for LEC-9 film. Larch bark extract promoted interactions with the polar groups of chitosan, resulting in accessibility of less number of polar groups to interact with water, thus leading to lower swelling of LEC films (Wang et al., 2019). On the other hand, the solubility increased considerably ($p < 0.05$) from 16.77% for PC to 25.79% for LEC-9. This would be quite expected from the hydrophilic character of polyphenols that enhanced the solubility of LEC films; although, their solubility did not differ significantly ($p > 0.05$) from each other.

The permeability reflects a crucial function of a film to act as a barrier to water vapor for food preservation. Interestingly, no significant differences ($p > 0.05$) were found in the permeability of chitosan films on incorporation of bark extract, with WVP ranging from 2.18×10^{-12} to 2.72×10^{-12} $gs^{-1}m^{-1}Pa^{-1}$. These values were, however, lower (and thus better) than those reported for chitosan films containing eggplant extract (Yong et al., 2019), mango leaf extract (Rambabu et al., 2019), thinned apple extract (Sun et al., 2017) and tea extracts (Peng et al., 2013). This may have resulted from the variations in factors affecting WVP viz., type of extract and plasticizer content of the film as well as the test conditions (temperature and humidity) (Rambabu et al., 2019).

The mechanical properties give fundamental insights into the behavior of a material for its practical use. The tensile strength, a measure of the maximum stress a film can withstand, was not significantly different ($p > 0.05$) for pristine and modified films except for LEC-3. The somewhat lower tensile strength of LEC films may be attributed to the reduction in crystallinity caused by the incorporation of polyphenols into the chitosan matrix (Sun et al., 2017). The polyphenols can interrupt the crystalline order in the polymer structure to weaken the intermolecular bonding and hamper chitosan chain interactions, thereby

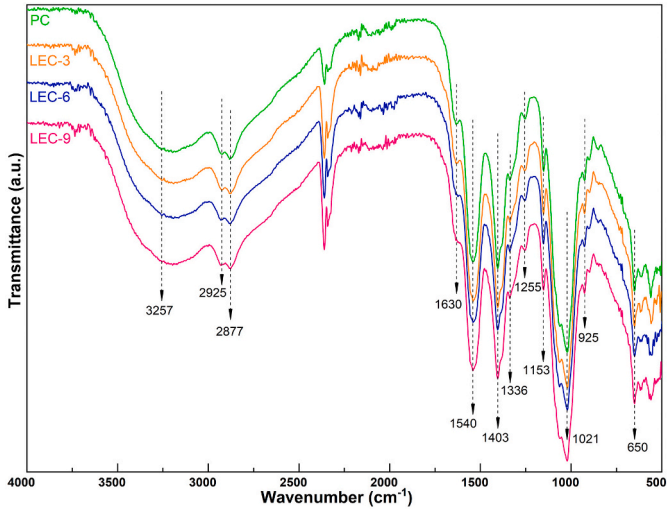

Fig. 3. FTIR spectra of pristine chitosan (PC) and larch bark extract-functionalized films. LEC-3, LEC-6 and LEC-9 represent chitosan films with 3 wt%, 6 wt% and 9 wt% larch bark extract concentration, respectively.

Table 1
Optical properties of pristine chitosan and larch bark extract-functionalized chitosan films.

Film code[#]	L*	a*	b*	ΔE	Chroma	Hue	Opacity
PC	93.56 ± 0.21^{d}	−0.37 ± 0.03^{a}	4.54 ± 0.08^{a}	0^{a}	4.56 ± 0.09^{a}	94.61 ± 0.37^{d}	2.21 ± 0.21^{a}
LEC-3	85.19 ± 1.03^{c}	5.62 ± 0.89^{b}	21.28 ± 2.04^{b}	19.65 ± 2.54^{b}	22.01 ± 2.20^{b}	75.25 ± 0.87^{c}	3.26 ± 0.45^{a}
LEC-6	78.70 ± 1.31^{b}	10.82 ± 1.08^{c}	32.31 ± 1.68^{c}	33.42 ± 2.16^{c}	34.08 ± 1.91^{c}	71.51 ± 0.95^{b}	5.95 ± 3.23^{a}
LEC-9	73.20 ± 1.57^{a}	15.97 ± 1.51^{d}	39.16 ± 2.63^{d}	43.35 ± 3.40^{d}	42.29 ± 3.00^{d}	67.84 ± 0.54^{a}	6.64 ± 2.10^{a}

Values are expressed as mean ± standard deviation. Different superscript letters within the same column indicate significant differences between means ($p < 0.05$).

[#] The film codes PC, LEC-3, LEC-6 and LEC-9 represent pristine chitosan and chitosan films with 3 wt%, 6 wt%, 9 wt% larch bark extract concentration, respectively.

lowering the tensile strength (Kadam et al., 2018; Sun et al., 2017). The elongation at break, which represents the stretch ability of a film prior to break, showed significant decline ($p < 0.05$) from 81.04% for PC to 24.32% for LEC-9. This indicated that addition of the extract appreciably enhanced the stiffness of LEC films and reduced the flexibility. The strong nature of LEC films can be understood from their much improved stiffness at comparable tensile strength compared to PC film. This overall improvement in the mechanical performance of LEC films resulted from the interactions between the extract constituents and chitosan, which has also been reported for thyme (Talón et al., 2017) and mango leaf (Rambabu et al., 2019) extracts.

3.6. Thermal analysis

The influence of larch bark extractives on the thermal degradation behavior of chitosan was analyzed by simultaneous TG-DSC measurements. As seen from the TG thermograms in Fig. 4a, the weight loss in all the films occurred in three major stages summarized in Table 3. The first stage event occurred in the temperature range of 40–140 °C, with a minor weight loss of 10–13%, primarily due to the loss of moisture bound in the hydroxyl and amino groups of chitosan (Rodrigues et al., 2020). The second stage event in the range of 140–240 °C, with a weight loss of 14–17% could be due to the degradation of glycerol (Almazrouei et al., 2019). The final stage event occurred in the range of 240–700 °C, contributing to a significant weight loss of 42–44%. This could be attributed to the complex decomposition of the acetylated and deacetylated units of chitosan (Liu et al., 2014). The total degradation was the highest for PC film, and the least for LEC-9 film having the highest extract content. About 26–32% char residue was left after 700 °C, which represented the ash content resulting from the thermal degradation of chitosan and bark extractives. The thermal events could be observed better in the derivative thermogravimetric (DTG) curves shown in Fig. 4b. The DTG plot shows the rate of weight loss and the peak temperature at which the decomposition rate is the highest. Clearly, PC film exhibited the highest rate of thermal degradation that reduced with increasing concentration of the extract in the films. However, the DTG peak temperature (T_{max}) corresponding to the maximum rate of thermal degradation (Table 3) was found to drop by few degrees for LEC films.

A further assessment in the thermal properties of the films was done with DSC thermograms, shown in Fig. 4c. The peak temperatures and enthalpy changes (ΔH) in the endothermic and exothermic phases are presented in Table 4. All the films exhibited two prominent peaks, one in the endothermic phase and the other in the exothermic phase. The endothermic peak at around 105 °C could be ascribed to the evaporation of solvents (water, acetic acid and ethanol) used during film preparation (Rodrigues et al., 2020). A broad shoulder seen around 160–180 °C in the endothermic region may be due to the denaturation of glycerol and extract constituents (Kaya et al., 2018). It should be noted here that the plasticizer and acetic acid tend to reduce the endothermic peak temperature of chitosan films (Peng et al., 2013). On the other hand, the exothermic peak at around 305 °C corresponds to the pyrolytic depolymerization and structural degradation of the chitosan backbone (Rodrigues et al., 2020). As evident from Table 4, the degradation peak temperature (T_{dg}) and enthalpy (ΔH_{dg}) reduced with increasing extract content. Thus, it can be concluded that larch bark extract negatively influenced the thermal stability of chitosan films. This can be attributed

Table 2
Physical and mechanical properties of pristine chitosan and larch bark extract-functionalized chitosan films.

Film code[#]	Thickness, mm	Density, g/cm^3	Moisture content, %	Swelling, %	Solubility, %	WVP, $\times 10^{-12}$ g s^{-1} m^{-1} Pa^{-1}	Tensile strength, MPa	Elongation at break, %
PC	0.062 ± 0.003^{a}	0.65 ± 0.09^{a}	14.69 ± 1.87^{b}	2752 ± 213^{c}	16.77 ± 0.14^{a}	2.18 ± 0.11^{a}	36.43 ± 3.11^{b}	81.04 ± 9.08^{b}
LEC-3	0.062 ± 0.002^{a}	0.92 ± 0.24^{a}	11.23 ± 1.37^{a}	590 ± 44^{b}	27.38 ± 4.21^{b}	2.72 ± 0.21^{a}	25.56 ± 2.82^{a}	40.00 ± 1.89^{a}
LEC-6	0.062 ± 0.001^{a}	1.21 ± 0.33^{a}	11.76 ± 0.49^{ab}	344 ± 50^{a}	24.56 ± 0.61^{b}	2.58 ± 0.51^{a}	34.40 ± 3.07^{b}	26.83 ± 5.95^{a}
LEC-9	0.061 ± 0.001^{a}	1.38 ± 0.65^{a}	10.29 ± 0.11^{a}	217 ± 38^{a}	25.79 ± 0.84^{b}	2.48 ± 0.38^{a}	30.98 ± 1.91^{ab}	24.32 ± 0.55^{a}

Values are expressed as mean ± standard deviation. Different superscript letters within the same column indicate significant differences between means ($p < 0.05$).

[#] The film codes PC, LEC-3, LEC-6 and LEC-9 represent pristine chitosan and chitosan films with 3 wt%, 6 wt%, 9 wt% larch bark extract concentration, respectively.

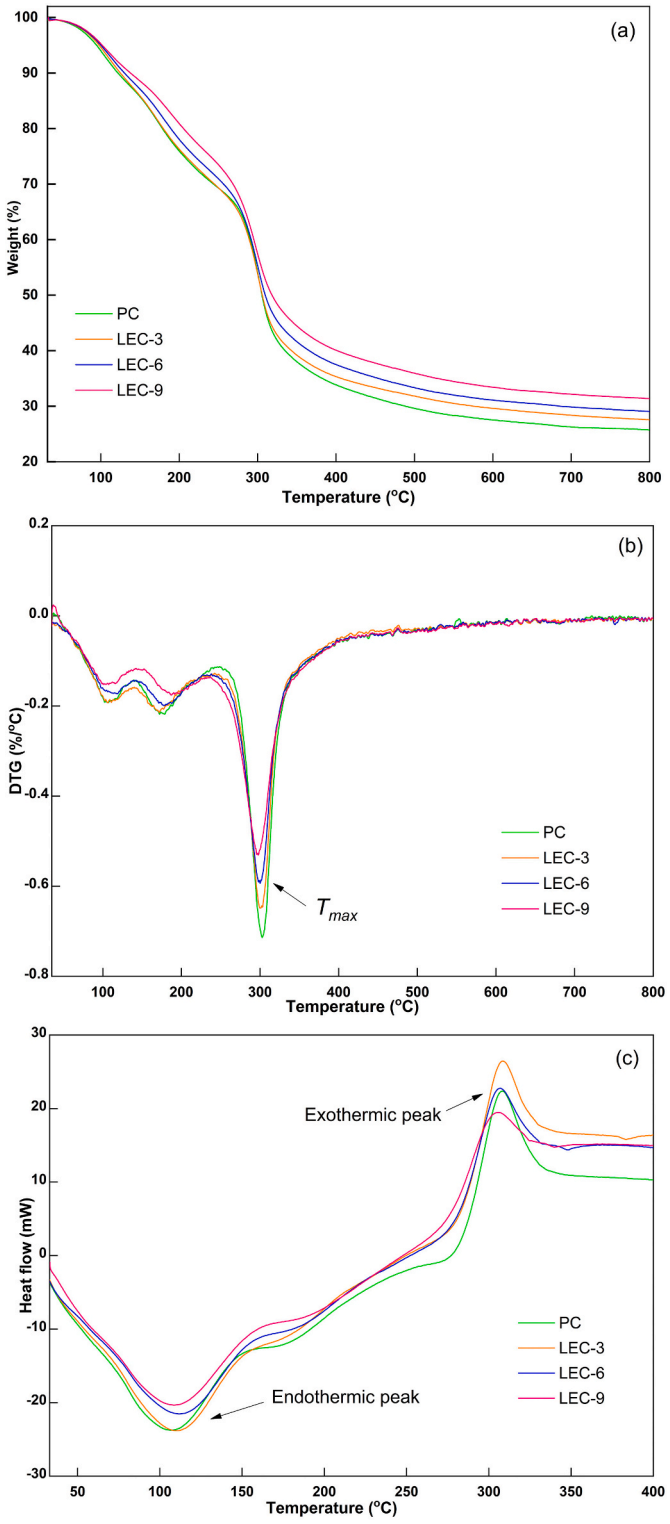

Fig. 4. (a) TG, (b) DTG and (c) DSC thermograms of pristine chitosan (PC) and larch bark extract-functionalized films. LEC-3, LEC-6 and LEC-9 represent chitosan films with 3 wt%, 6 wt% and 9 wt% larch bark extract concentration, respectively.

to bond and chain scission resulting from incorporation of the extract, causing disruption in the crystalline regions of the polymer structure and subsequent drop in the thermal stability (Kaya et al., 2018). Similar thermal behavior of chitosan films modified with plant extracts has also been found in earlier studies (Kaya et al., 2018; Peng et al., 2013; Sun et al., 2017).

Table 3
TG and DTG results for pristine chitosan and larch bark extract-functionalized chitosan films.

Film code[#]	TG weight loss, %				DTG peak (T_{max}), °C
	Stage 1	Stage 2	Stage 3	Total	
PC	12.7	16.8	44.2	73.7	302.8
LEC-3	12.5	17.0	42.1	71.6	301.4
LEC-6	11.4	16.3	42.4	70.1	299.9
LEC-9	10.2	14.8	42.8	67.8	296.9

[#] The film codes PC, LEC-3, LEC-6 and LEC-9 represent pristine chitosan and chitosan films with 3 wt%, 6 wt%, 9 wt% larch bark extract concentration, respectively.

Table 4
DSC values for peak temperature and enthalpy for pristine chitosan and larch bark extract-functionalized chitosan films.

Film code[#]	Endothermic phase		Exothermic phase	
	Dehydration temperature (T_{dh}), °C	Dehydration enthalpy (ΔH_{dh}), J/g	Degradation temperature (T_{dg}), °C	Degradation enthalpy (ΔH_{dg}), J/g
PC	104.6	233.3	308.7	217.8
LEC-3	109.1	214.7	309.3	294.1
LEC-6	111.0	218.7	307.2	160.3
LEC-9	108.1	225.9	305.0	106.4

[#] The film codes PC, LEC-3, LEC-6 and LEC-9 represent pristine chitosan and chitosan films with 3 wt%, 6 wt%, 9 wt% larch bark extract concentration, respectively.

3.7. Dynamic mechanical analysis

The viscoelastic properties of pristine and extract-functionalized chitosan films were investigated by DMA curves. Fig. 5 illustrates the storage modulus (E′), loss modulus (E″) and tan δ (E″/E′) as a function of temperature.

The storage modulus represents the energy storage capacity of the film and is a measure of its elastic behavior. The storage modulus increased with the addition of bark extractives (Fig. 5a), where the highest value was shown by LEC-9 film. The increase in storage modulus at higher extract concentrations may be due to interactions between bark extractives and chitosan causing conformational changes (Boonsongrit et al., 2008). At higher storage modulus, the polymer chain mobility is more restricted, thus resulting in a lower elongation at break. This was in agreement with the results in Table 2, showing LEC-9 film with the highest extract content having the least elongation at break, although not significantly different from LEC-3 and LEC-6 films. Similar behavior in DMA patterns has been reported earlier (Thakhiew et al., 2013). A steep decline in storage modulus from around 90 °C to 150 °C was observed for all the films. This region signifies the transition from a glassy (rigid) state to a rubbery (flexible) state caused by increasing mobility of the polymer matrix.

The loss modulus represents the heat loss capacity of the film and is a measure of its viscose behavior. It showed a similar trend (Fig. 5b) as storage modulus, with LEC-9 film exhibiting the highest value. In general, a higher loss modulus is linked to a higher tensile strength, as observed earlier (M. Liu et al., 2014). However, the tensile strength of the films (Table 2) did not increase with extract concentration. This may be due to the counterbalancing effect of the reduced crystallinity at higher extract concentrations (Thakhiew et al., 2013).

The tan δ (damping) curve represents the dissipation of energy in the film and is used to determine the glass transition temperature (T_g). The T_g is determined from the peak in the tan δ curve in the maximum declining range of the storage modulus (Tuhin et al., 2012). As evident from Fig. 5c, the tan δ peak height increased with extract content

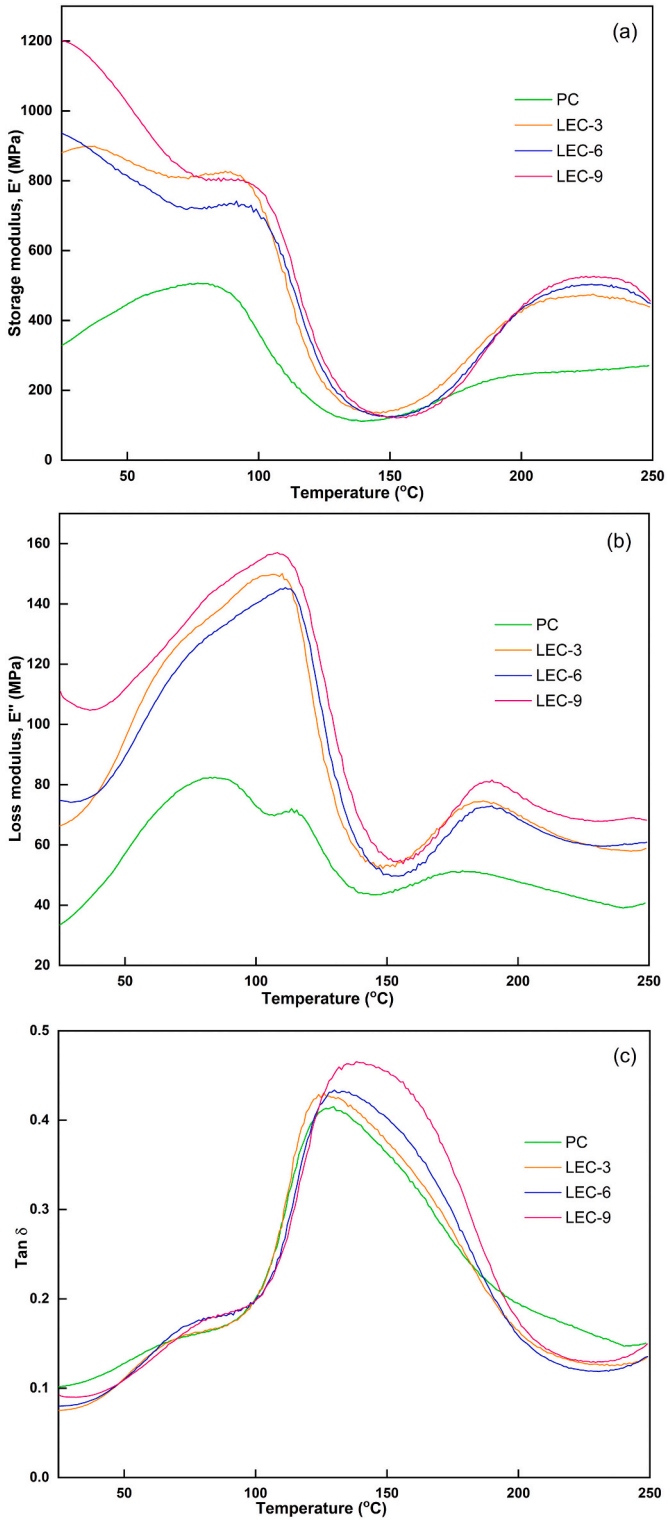

Fig. 5. (a) Storage modulus, (b) loss modulus and (c) tan δ of pristine chitosan (PC) and larch bark extract-functionalized films. LEC-3, LEC-6 and LEC-9 represent chitosan films with 3 wt%, 6 wt% and 9 wt% larch bark extract concentration, respectively.

indicating its enhanced chain mobility or flexibility. The LEC-9 film had the highest tan δ peak with T_g of 138.2 °C, LEC-6 had T_g of 129.9 °C, and LEC-3 had T_g of 126.1 °C. Nevertheless, the increased flexibility effect appears to have been masked, as indicated by an increase in T_g of LEC-9 compared to PC film with T_g of 129.7 °C, thus resulting in lower chain mobility. Additionally, all films with bark extractives showed a much higher storage modulus compared to PC film as already mentioned. This synergistic lowering effect can be confirmed from the significantly lower elongation at break values of LEC films, as given in Table 2. Notably, the presence of glycerol in the chitosan films lowered the T_g due to plasticizing effect that led to reduction in intermolecular forces (Prateepchanachai et al., 2017).

3.8. Antioxidant capacity analysis

The TPC and DPPH radical scavenging results are depicted in Fig. 6. The TPC assay measures the total reducing capacity of the sample, and not merely the phenolic profile (Baldan et al., 2017). The reducing compounds in the film including polyphenols can give a good estimate of its antioxidant potential, as they have the ability to donate H^+ ions from the –OH groups and delocalize free electrons (Rambabu et al., 2019). It can be seen from Fig. 6a that the phenolic content increased significantly ($p < 0.05$) with increasing concentration of larch bark extract in the films. A low phenolic content in the control PC film was probably due to the presence of chromogens (Liu et al., 2017). Nearly 10-fold rise in TPC was achieved in case of LEC-9 film (894 mg GAE/g dw) compared to PC film (90 mg GAE/g dw). The phenomenal increase in phenolic content in LEC films can be attributed to the presence of larch bark extractives, indicating that the extract is rich in phenolic compounds. Apart from polyphenols, larch bark also contains bioactive compounds such as procyanidins and flavonoids (Agarwal, Hofmann, Vršanská, et al., 2021).

Since the antioxidant assays are strongly influenced by the extract constituents; many complementary methods are used in antioxidant studies. The DPPH radical scavenging assay is widely used in the quantitative assessment of antioxidants. It is based on the quenching of

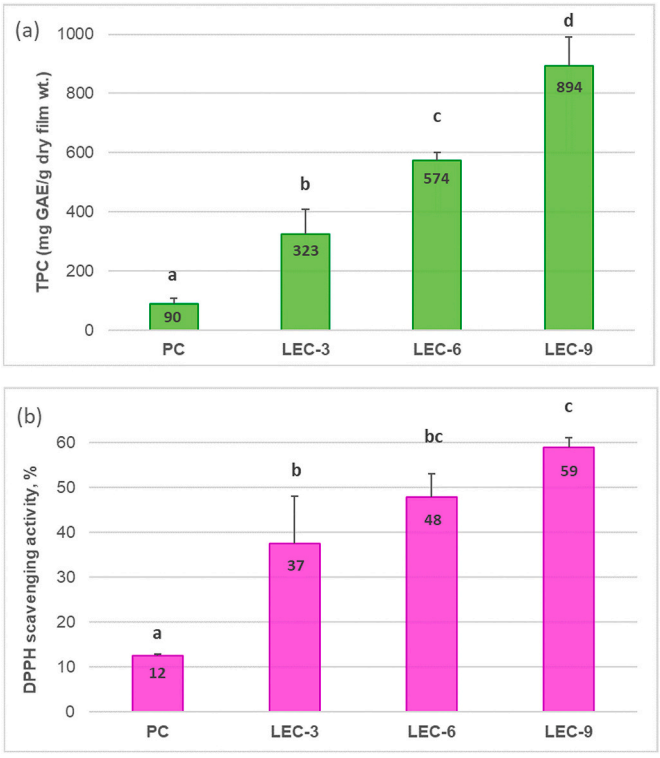

Fig. 6. (a) Total phenol content (TPC) and (b) DPPH radical scavenging activity of pristine chitosan (PC) and larch bark extract-functionalized chitosan films. LEC-3, LEC-6 and LEC-9 represent chitosan films with 3 wt%, 6 wt% and 9 wt% larch bark extract concentration, respectively. The values are expressed as mean ± standard deviation and different letters indicate significant differences between means ($p < 0.05$).

DPPH free radicals by the antioxidants in the extract resulting in a color change from purple to pale yellow and a drop in absorbance. As clear from Fig. 6b, DPPH radical scavenging activity of the films was significantly ($p < 0.05$) enhanced in the presence of the extract. Interestingly, the control film also had scavenging effect from the free amino groups in chitosan (Siripatrawan & Harte, 2010). Maximum scavenging activity of 59% was obtained for LEC-9 film, which was almost 5 times more than that of PC film. The scavenging activity increased with the extract concentration, also indicating the antioxidant nature of bark extractives incorporated in the films. A strong correlation ($r = 0.96$) was found between TPC and DPPH radical scavenging activity of the films. Another study using green tea extract in chitosan reported similar findings (Siripatrawan & Harte, 2010).

4. Conclusion

Natural bioactive compounds extracted from the whole bark of larch were functionalized onto chitosan to develop active packaging films. Influence of the incorporation of bark extractives was analyzed on various properties of pristine and modified chitosan films containing 3, 6 and 9 wt% extract. The structural analyses revealed non-covalent interactions between the chitosan matrix and polyphenolic compounds with good compatibility between them. Compared to pristine chitosan, LEC films demonstrated an increase in solubility, with a significant drop in swelling and elongation at break. Increasing opacity of the films indicated a rising trend in the visible light barrier with addition of the extract. However, the tensile strength did not improve significantly on addition of the extract, probably due to reduced crystallinity. The LEC films showed a remarkable enhancement in antioxidant activity due to the presence of polyphenolic compounds from bark. On the whole, LEC films demonstrated promise as active food packaging material. They could be potentially used in packaging of fresh fruits and vegetables, as well as bakery and confectionery items. This work demonstrated larch bark as a rich source of natural antioxidants with immense potential in active packaging. It will encourage the exploration and utilization of secondary biomass-derived extracts for the development of sustainable packaging materials.

CRediT authorship contribution statement

Charu Agarwal: Conceptualization, Formal analysis, Validation, Writing – original draft. **Zsófia Kóczán:** Methodology, Investigation. **Zoltán Börcsök:** Investigation. **Katalin Halász:** Methodology, Writing – review & editing. **Zoltán Pásztory:** Supervision, Project administration.

Declaration of competing interest

There are no competing interests to declare.

Acknowledgments

The work was carried out as part of the “Sustainable raw material management thematic network – RING 2017”, EFOP-3.6.2-16-2017-00010 project in the framework of the Széchenyi 2020 Program. The realization of this project is supported by the European Union, co-financed by the European Social Fund.

References

Agarwal, C., Hofmann, T., Visi-Rajczi, E., & Pásztory, Z. (2021). Low-frequency, green sonoextraction of antioxidants from tree barks of Hungarian woodlands for potential food applications. *Chemical Engineering and Processing Process Intensification, 159*, Article 108221. https://doi.org/10.1016/j.cep.2020.108221

Agarwal, C., Hofmann, T., Vršanská, M., Schlosserová, N., Visi-Rajczi, E., Voběrková, S., & Pásztory, Z. (2021). In vitro antioxidant and antibacterial activities with polyphenolic profiling of wild cherry, the European larch and sweet chestnut tree bark. *European Food Research and Technology*. https://doi.org/10.1007/s00217-021-03796-w

Almazrouei, M., Elagroudy, S., & Janajreh, I. (2019). Transesterification of waste cooking oil: Quality assessment via thermogravimetric analysis. *Energy Procedia, 158*, 2070–2076. https://doi.org/10.1016/j.egypro.2019.01.478

Assis, R. Q., Rios, P. D. A., Rios, A.d. O., & Olivera, F. C. (2020). Biodegradable packaging of cellulose acetate incorporated with norbixin, lycopene or zeaxanthin. *Industrial Crops and Products, 147*(February), Article 112212. https://doi.org/10.1016/j.indcrop.2020.112212

ASTM International. (2016). *ASTM E96/E96M-16, Standard test methods for water vapor transmission of materials*. https://doi.org/10.1520/E0096_E0096M-16

Baldan, V., Sut, S., Faggian, M., Gassa, E. D., Ferrari, S., De Nadai, G., … Dall'Acqua, S. (2017). Larix decidua bark as a source of phytoconstituents: An LC-MS study. *Molecules, 22*(11), 1–14. https://doi.org/10.3390/molecules22111974

Boonsongrit, Y., Mueller, B. W., & Mitrevej, A. (2008). Characterization of drug-chitosan interaction by 1H NMR, FTIR and isothermal titration calorimetry. *European Journal of Pharmaceutics and Biopharmaceutics, 69*(1), 388–395. https://doi.org/10.1016/j.ejpb.2007.11.008

Etxabide, A., Uranga, J., Guerrero, P., & de la Caba, K. (2017). Development of active gelatin films by means of valorisation of food processing waste: A review. *Food Hydrocolloids, 68*, 192–198. https://doi.org/10.1016/j.foodhyd.2016.08.021

FAO. (2014). *Appropriate food packaging solutions for developing countries*.

FAO. (2021). Food loss and food waste. http://www.fao.org/food-loss-and-food-waste/flw-data.

FAO, IFAD, UNICEF, WFP, & WHO. (2020). *The State of Food Security and Nutrition in the World 2020. Transforming food systems for affordable healthy diets*. https://doi.org/10.4060/ca9692en

Ferreira, A. S., Nunes, C., Castro, A., Ferreira, P., & Coimbra, M. A. (2014). Influence of grape pomace extract incorporation on chitosan films properties. *Carbohydrate Polymers, 113*, 490–499. https://doi.org/10.1016/j.carbpol.2014.07.032

Halász, K., & Csóka, L. (2018). Black chokeberry (Aronia melanocarpa) pomace extract immobilized in chitosan for colorimetric pH indicator film application. *Food Packaging and Shelf Life, 16*(April), 185–193. https://doi.org/10.1016/j.fpsl.2018.03.002

Jeevahan, J., & Chandrasekaran, M. (2019). Nanoedible films for food packaging: A review. *Journal of Materials Science, 54*(19), 12290–12318. https://doi.org/10.1007/s10853-019-03742-y

Kadam, D., Shah, N., Palamthodi, S., & Lele, S. S. (2018). An investigation on the effect of polyphenolic extracts of Nigella sativa seedcake on physicochemical properties of chitosan-based films. *Carbohydrate Polymers, 192*, 347–355. https://doi.org/10.1016/j.carbpol.2018.03.052

Kalaycıoğlu, Z., Torlak, E., Akın-Evingür, G., Özen, İ., & Erim, F. B. (2017). Antimicrobial and physical properties of chitosan films incorporated with turmeric extract. *International Journal of Biological Macromolecules, 101*, 882–888. https://doi.org/10.1016/j.ijbiomac.2017.03.174

Kaya, M., Khadem, S., Cakmak, Y. S., Mujtaba, M., Ilk, S., Akyuz, L., … Deligöz, E. (2018). Antioxidative and antimicrobial edible chitosan films blended with stem, leaf and seed extracts of Pistacia terebinthus for active food packaging. *RSC Advances, 8*(8), 3941–3950. https://doi.org/10.1039/c7ra12070b

Liu, J., Liu, S., Wu, Q., Gu, Y., Kan, J., & Jin, C. (2017). Effect of protocatechuic acid incorporation on the physical, mechanical, structural and antioxidant properties of chitosan film. *Food Hydrocolloids, 73*, 90–100. https://doi.org/10.1016/j.foodhyd.2017.06.035

Liu, M., Zhou, Y., Zhang, Y., Yu, C., & Cao, S. (2014). Physicochemical, mechanical and thermal properties of chitosan films with and without sorbitol. *International Journal of Biological Macromolecules, 70*, 340–346. https://doi.org/10.1016/j.ijbiomac.2014.06.039

Lourenço, S. C., Moldão-Martins, M., & Alves, V. D. (2019). Antioxidants of natural plant origins: From sources to food industry applications. *Molecules, 24*(22), 14–16. https://doi.org/10.3390/molecules24224132

Park, S. I., & Zhao, Y. (2004). Incorporation of a high concentration of mineral or vitamin into chitosan-based films. *Journal of Agricultural and Food Chemistry, 52*(7), 1933–1939. https://doi.org/10.1021/jf034612p

Peng, Y., Wu, Y., & Li, Y. (2013). Development of tea extracts and chitosan composite films for active packaging materials. *International Journal of Biological Macromolecules, 59*, 282–289. https://doi.org/10.1016/j.ijbiomac.2013.04.019

Prateepchanachai, S., Thakhiew, W., Devahastin, S., & Soponronnarit, S. (2017). Mechanical properties improvement of chitosan films via the use of plasticizer, charge modifying agent and film solution homogenization. *Carbohydrate Polymers, 174*, 253–261. https://doi.org/10.1016/j.carbpol.2017.06.069

Rambabu, K., Bharath, G., Banat, F., Show, P. L., & Cocoletzi, H. H. (2019). Mango leaf extract incorporated chitosan antioxidant film for active food packaging. *International Journal of Biological Macromolecules, 126*, 1234–1243. https://doi.org/10.1016/j.ijbiomac.2018.12.196

Rodrigues, C., de Mello, J. M. M., Dalcanton, F., Macuvele, D. L. P., Padoin, N., Fiori, M. A., … Riella, H. G. (2020). Mechanical, thermal and antimicrobial properties of chitosan-based-nanocomposite with potential applications for food packaging. *Journal of Polymers and the Environment, 28*(4), 1216–1236. https://doi.org/10.1007/s10924-020-01678-y

Sanches-Silva, A., Costa, D., Albuquerque, T. G., Buonocore, G. G., Ramos, F., Castilho, M. C., … Costa, H. S. (2014). Trends in the use of natural antioxidants in active food packaging: A review. *Food Additives and Contaminants - Part A Chemistry, Analysis, Control, Exposure and Risk Assessment, 31*(3), 374–395. https://doi.org/10.1080/19440049.2013.879215

Siripatrawan, U., & Harte, B. R. (2010). Physical properties and antioxidant activity of an active film from chitosan incorporated with green tea extract. *Food Hydrocolloids, 24*(8), 770–775. https://doi.org/10.1016/j.foodhyd.2010.04.003

Souza, V. G. L., Fernando, A. L., Pires, J. R. A., Rodrigues, P. F., Lopes, A. A. S., & Fernandes, F. M. B. (2017). Physical properties of chitosan films incorporated with natural antioxidants. *Industrial Crops and Products, 107*(May), 565–572. https://doi.org/10.1016/j.indcrop.2017.04.056

Sun, L., Sun, J., Chen, L., Niu, P., Yang, X., & Guo, Y. (2017). Preparation and characterization of chitosan film incorporated with thinned young apple polyphenols as an active packaging material. *Carbohydrate Polymers, 163*, 81–91. https://doi.org/10.1016/j.carbpol.2017.01.016

Talón, E., Trifkovic, K. T., Nedovic, V. A., Bugarski, B. M., Vargas, M., Chiralt, A., & González-Martínez, C. (2017). Antioxidant edible films based on chitosan and starch containing polyphenols from thyme extracts. *Carbohydrate Polymers, 157*, 1153–1161. https://doi.org/10.1016/j.carbpol.2016.10.080

Thakhiew, W., Devahastin, S., & Soponronnarit, S. (2013). Physical and mechanical properties of chitosan films as affected by drying methods and addition of antimicrobial agent. *Journal of Food Engineering, 119*(1), 140–149. https://doi.org/10.1016/j.jfoodeng.2013.05.020

Tuhin, M. O., Rahman, N., Haque, M. E., Khan, R. A., Dafader, N. C., Islam, R., … Tonny, W. (2012). Modification of mechanical and thermal property of chitosan-starch blend films. *Radiation Physics and Chemistry, 81*(10), 1659–1668. https://doi.org/10.1016/j.radphyschem.2012.04.015

Vilela, C., Kurek, M., Hayouka, Z., Röcker, B., Yildirim, S., Antunes, M. D. C., … Freire, C. S. R. (2018). A concise guide to active agents for active food packaging. *Trends in Food Science and Technology, 80*(August), 212–222. https://doi.org/10.1016/j.tifs.2018.08.006

Wang, L., Guo, H., Wang, J., Jiang, G., Du, F., & Liu, X. (2019). Effects of Herba Lophatheri extract on the physicochemical properties and biological activities of the chitosan film. *International Journal of Biological Macromolecules, 133*, 51–57. https://doi.org/10.1016/j.ijbiomac.2019.04.067

Yong, H., Wang, X., Zhang, X., Liu, Y., Qin, Y., & Liu, J. (2019). Effects of anthocyanin-rich purple and black eggplant extracts on the physical, antioxidant and pH-sensitive properties of chitosan film. *Food Hydrocolloids, 94*(January), 93–104. https://doi.org/10.1016/j.foodhyd.2019.03.012

Zhong, Y., Godwin, P., Jin, Y., & Xiao, H. (2020). Biodegradable polymers and green-based antimicrobial packaging materials: A mini-review. *Advanced Industrial and Engineering Polymer Research, 3*(1), 27–35. https://doi.org/10.1016/j.aiepr.2019.11.002